International Journal of Solids and Structures 46 (2009) 3516–3534

Contents lists available at ScienceDirect

International Journal of Solids and Structures

journal homepage: www.elsevier.com/locate/ijsolstr

Nonlocal damage theory in hybrid-displacement formulations

C.M. Silva, L.M.S.S. Castro *

Departamento de Engenharia Civil e Arquitectura, Instituto Superior Técnico, Avenida Rovisco Pais, 1049-001 Lisbon, Portugal

ARTICLE INFO

Article history:
Received 23 December 2008
Received in revised form 1 April 2009
Available online 15 May 2009

Keywords:
Nonlocal damage models
Hybrid-displacement formulations
Legendre polynomials
Trefftz functions

ABSTRACT

This paper discusses three hybrid-displacement finite element formulations for the simulation of strain localization based on nonlocal damage theory. An isotropic integral nonlocal damage model is chosen. The hybrid finite element formulations adopted in this work are developed from first principles of Mechanics. The first one defines the domain approximations using the Trefftz functions derived for the linear elastic regime. When damage appears the hybrid-Trefftz displacement formulation degenerates into an hybrid-displacement formulation. The second formulation uses an enriched Trefftz basis with the consideration of local Heaviside functions. The third formulation uses orthonormal Legendre polynomials for the domain approximations. A set of benchmark tests is presented and discussed in order to compare the performance and accuracy of the different models. It is shown that the proposed hybrid-Trefftz formulation allows the reproduction of the general behavior of the structure but does not lead to a correct simulation of the strain tensor evolution. The hybrid-displacement formulation that uses orthonormal Legendre polynomials gives coherent results, so it appears to be a promising field of investigation.

1. Introduction

The hybrid-displacement models adopted in this work are based on the non-conventional finite element models developed by Freitas et al. (1999a). According to this author, these formulations may be classified into three main classes, in particular the hybrid-mixed, the hybrid and the hybrid-Trefftz formulation. Two models are derived for each formulation, the displacement and the stress model (Castro, 1996; Wang, 2000; Cismaşiu, 2000). All the formulations evolve directly from the first principles of Mechanics, namely equilibrium, compatibility and constitutive relations (Section 2). What distinguishes the three types of formulations is the set of constraints enforced, *a priori*, on the domain approximations.

In the hybrid-displacement formulations, only the compatibility in the domain is enforced *a priori*. All remaining field equations are imposed in a weighted-residual form, ensuring that the discrete numerical model embodies all the relevant properties of the continuum fields it represents. The displacements in the domain of each element and the tractions on the kinematic boundary, which is considered to include the inter-element boundaries, are independently approximated.

During the nineties, the accuracy and numerical performance of these non-conventional models for linear elastic analysis were assessed. Several advantages may be associated with these formulations, namely the possibility of defining macro-elements and introducing easily a *p*-refinement based on the increase of polynomial order of finite element shape functions. It has been show that the hybrid-Trefftz displacement formulation is one of the most promising models. The main feature of this formulation is that the functions used to approximate the displacements are derived from bi-harmonic displacement potentials that solve the Navier equations for a homogeneous elastic material (Freitas et al., 1999b; Cismaşiu, 2000). Consequently, the accuracy of the solution may be very good even using a small number of degrees of freedom.

In recent years, some of these non-conventional finite element formulations have been extended to nonlinear analysis using isotropic damage models (Silva and Castro, 2005, 2006, 2007). Since the Trefftz model is one of the most competitive formulations in the linear elastic regime, the first step is to test its performance for the nonlinear elastic regime. The main drawback of using this formulation with continuum damage models is the definition of the approximation functions. In the nonlinear elastic regime, it is difficult to define approximation functions that satisfy the Trefftz condition. Therefore, the functions of the linear elastic regime are chosen. When damage appears, the hybrid(-Trefftz) displacement formulation degenerates into a hybrid-displacement formulation. Although in the fracture process zone the approximation functions do not englobe all the necessary information, since the approximation functions are forced to verify the Trefftz condition of the linear elastic regime, it is expected that the model can simulate correctly the global

* Corresponding author. Tel.: +351 218418253; fax: +351 218497650.
E-mail addresses: luis@civil.ist.utl.pt, luissantoscastro@gmail.com (L.M.S.S. Castro).

0020-7683/$ - see front matter © 2009 Elsevier Ltd. All rights reserved.
doi:10.1016/j.ijsolstr.2009.05.004

behavior with few degrees of freedom. On the other hand, this choice is reasonable since it is known that localization appears and develops in a small part of the domain and that linear behavior still holds in most part of the structure, where the advantages of the pure hybrid-Trefftz formulation are valid.

In this paper, it is shown that the hybrid(-Trefftz) formulation simulates correctly the global behavior of the structure with damage but does not approximate with enough precision the evolution of the strain field. Therefore, a second formulation is considered, corresponding to an enriched Trefftz basis with the consideration of local Heaviside functions. This type of functions has also been applied by Patzák and Jirásek (2003) in the context of extended finite elements. This second approach improves the description of the evolving strain profile, by adding only a few number of degrees of freedom. However, the definition and computational treatment of such local approximation functions in multiple dimensions would be quite difficult.

Finally, the numerical performance of a hybrid-displacement finite element model using orthonormal Legendre polynomials for both the domain and boundary approximations is evaluated. This third model is computationally more demanding but overcomes the drawbacks found in the previous models.

All three hybrid-displacement models described here exhibit most of the main advantages found in the linear elastic regime for these non-conventional formulations, as the possibility of using macro-elements and attractive *p*-refinement techniques. The main objective of this paper is to present and discuss three variants of the hybrid-displacement model for nonlinear analysis using continuum damage models and compare their relative performance, in order to choose one approach for further developments.

The nonlinear behavior of the structural material is modeled assuming an isotropic continuum damage model. Continuum damage mechanics is an important tool that describes the evolution of the mechanical properties of the continuum as micro cracking develops (Lemaitre, 1992; LaBorderie, 1991; Mazars and Pijaudier-Cabot, 1989; Comi and Perego, 2001a; Comi, 2001).

A strain softening material law is considered in order to be able to model a structural softening behavior. However, strain softening is well known to produce strain localization with consequent dependence on the data of the finite element model, as for instance the mesh and the degree of the approximation functions adopted (Bažant, 1976; Jirásek et al., 2001). To overcome this problem, several regularization techniques are proposed in the literature, in particular nonlocal integral (Pijaudier-Cabot and Bažant, 1987; Bažant and Jirásek, 2002) and gradient-enhanced damage formulations (Peerlings et al., 1996; Comi, 1999). Following (Comi and Perego, 2001b), the present work adopts a nonlocal integral model where the strain energy release rate is adopted as the nonlocal variable.

Only static and monotonic loads are considered and small strains and rotations are assumed. The numerical model adopted is both incremental and iterative. It was implemented in a C program and all tests were performed on a Pentium IV Machine running Linux.

This paper is organized as follows: the formulation of the problem and the adopted damage model are presented in Section 2. The hybrid-displacement finite element formulation is presented in Section 3 and the implementation details corresponding to the three variants are described in Section 4. Numerical examples are presented in Sections 5 and 6 to illustrate the application of the models and to characterize their performance. Finally, Section 7 presents the main conclusions and indicates future research work in this field.

2. Fundamental relations

Consider a domain V limited by the boundary Γ, referred to a cartesian coordinate system. The static boundary Γ_σ (Neumann boundary) and the kinematic boundary Γ_u (Dirichlet boundary) are complementary sub-regions of the boundary Γ, whereon traction-resultants and displacements are, respectively, prescribed. The static loads considered include the body-force vector $\mathbf{b}$ in the domain V, the tractions vector $\mathbf{t}_\gamma$ on the boundary Γ_σ, and the prescribed displacements on the kinematic boundary Γ_u defined in vector $\bar{\mathbf{u}}$.

2.1. Equilibrium and compatibility equations

The fundamental equilibrium equations may be written in a matrix form as follows:

$$\mathbf{D}\boldsymbol{\sigma} + \mathbf{b} = \mathbf{0} \quad \text{in } V, \tag{1}$$

$$\mathbf{N}\boldsymbol{\sigma} = \mathbf{t}_\gamma \quad \text{on } \Gamma_\sigma, \tag{2}$$

where $\mathbf{D}$ is the differential equilibrium operator. The matrix $\mathbf{N}$ contains the components of the unit outward normal vector to the static boundary Γ_σ associated with $\mathbf{D}$. The vector $\boldsymbol{\sigma}$ lists the independent components of the stress tensor.

The compatibility equations may be written in the following format:

$$\boldsymbol{\epsilon} = \mathbf{D}^*\mathbf{u} \quad \text{in } V, \tag{3}$$

$$\mathbf{u} = \bar{\mathbf{u}} \quad \text{on } \Gamma_u, \tag{4}$$

where $\mathbf{D}^*$ is the differential compatibility operator (adjoint of the differential equilibrium operator $\mathbf{D}$ since the model is geometrically linear). The vector $\boldsymbol{\epsilon}$ collects the independent components of the strain tensor and the vector $\mathbf{u}$ lists the independent components of the displacement field.

2.2. Nonlocal damage model

The isotropic damage model adopted here is based on the following definition for the free energy density potential (Comi and Perego, 2001c):

$$\Psi = \frac{1}{2}(1-d)\boldsymbol{\varepsilon}^t\mathbf{E}\boldsymbol{\varepsilon} + k(1-\xi)\sum_{i=0}^{n}\frac{n!}{i!}\ln^i\left(\frac{c}{1-\xi}\right), \tag{5}$$

where $\mathbf{E}$ corresponds to the elastic stiffness matrix of the virgin material and d is the isotropic damage variable. The second term represents the inelastic free energy density and is written in terms of a scalar internal variable of kinematic nature, ξ. The variables k, n and c are material parameters.

Using the Helmholtz free energy density defined in Eq. (5) and considering the fundamental principles of thermodynamics (Lemaitre, 1992), it is possible to obtain the following state equations:

$$\boldsymbol{\sigma} = \frac{\partial\Psi}{\partial\boldsymbol{\varepsilon}} = (1-d)\mathbf{E}\boldsymbol{\varepsilon}, \quad \chi = -\frac{\partial\Psi}{\partial\xi} = -\Psi'_{in}(\xi), \quad Y = -\frac{\partial\Psi}{\partial d} = \frac{1}{2}\boldsymbol{\varepsilon}^t\mathbf{E}\boldsymbol{\varepsilon}, \tag{6}$$

where $\boldsymbol{\varepsilon}, \xi$ and d are the state variables and $\boldsymbol{\sigma}, \chi$ and Y represent the corresponding associated variables. The evolution laws are obtained from the potential of dissipation, f, which is written in terms of the associated variables and defined in order to satisfy the Clausius–Duhem inequality (Lemaitre, 1992). Eq. (7) defines the potential of dissipation and the loading–unloading conditions:

$$f(Y-\chi) = Y - \chi = \frac{1}{2}\boldsymbol{\varepsilon}^t\mathbf{E}\boldsymbol{\varepsilon} - \chi \leqslant 0, \qquad \dot{\gamma} \geqslant 0, \qquad f\dot{\gamma} = 0, \tag{7}$$

where γ represents a positive scalar.

The evolution laws may be written in the following form:

$$\dot{d} = \frac{\partial f}{\partial Y}\dot{\gamma} = \dot{\gamma}, \qquad \dot{\xi} = -\frac{\partial f}{\partial \chi}\dot{\gamma} = \dot{\gamma}. \tag{8}$$

Analyzing Eq. (8), one concludes that, for this particular damage model, the internal variable ξ coincides with the damage variable d.

The adopted damage model has the limitation of considering the same behavior for the material in prevailing tension and compression states, which is not realistic for most materials. To overcome this limitation, it is assumed that damage may only appear if the trace of the strain tensor is positive, $tr\,\boldsymbol{\varepsilon} > 0$. The constitutive model with the referred assumption is suitable for studying structures subjected mainly to tension stresses and even competitive due to its simplicity.

A finite element analysis of materials with softening behavior is well known to localize strains in a vanishing volume and leads, consequently, to unrealistic solutions associated with zero energy dissipation, as described, e.g., in Bažant (1976). There are several possibilities to restore the well-posedness of this problem (see e.g., Bažant and Jirásek, 2002; Peerlings et al., 1996). In the present work, a nonlocal integral formulation is adopted.

Following (Pijaudier-Cabot and Bažant, 1987), the proposed model averages the damage energy release rate, Y in Eq. (6), considering a weighted average over the whole domain:

$$\overline{Y}(x) = \int_V W(x,s)Y(s)\,\mathrm{d}s, \tag{9}$$

where $W(x,s)$ is a weight function taken here as the normalized Gauss function:

$$W(x,s) = \frac{1}{W_0(x)}\exp\left(-\frac{\|x-s\|^2}{2l^2}\right),$$
$$W_0(x) = \int_V \exp\left(-\frac{\|x-s\|^2}{2l^2}\right)\mathrm{d}s. \tag{10}$$

The length l in Eq. (10) is a geometrical length, usually denoted as *characteristic length*. It works as a localization limiter and regularizes the mathematical problem. According to Bažant and Pijaudier-Cabot (1989), this length may also be interpreted as a material-dependent parameter related to the width of the fracture process zone. A normalized weight function is chosen because the nonlocal model should be able to reproduce correctly local uniform fields. The nonlocal model is obtained from the local model introducing in Eq. (7) the nonlocal value for the energy release rate, $\overline{Y}$ (Silva and Castro, 2004).

Performing an unidimensional wave propagation analysis, we obtain the following relation between the damage variable d and the nonlocal characteristic length, λ_c (Comi and Perego, 2001c):

$$\lambda_c = \sqrt{2}\pi l\left[-\ln\left(\frac{n}{2\ln\left(\frac{c}{1-d}\right)}\right)\right]^{-0.5}. \tag{11}$$

The nonlocal characteristic length defines the width of the zone in which damage tends to localize. It is proportional to the geometric parameter l but also depends on the particular formulation adopted and on the chosen weight function. As expected, λ_c is a decreasing function of d.

3. Hybrid-displacement formulation (Freitas et al., 1999a)

The hybrid-displacement finite element formulation adopted in this work is developed from first principles of Mechanics (Timoshenko and Goodier, 1970). Two independent approximations are defined, one for the displacement field, $\mathbf{u}$, in the domain of each finite element and the other to the tractions, $\mathbf{t}$, on the kinematic boundary, which includes the inter-element boundaries. The displacement continuity between elements is imposed in a weighted-residual form using the compatibility equation on Γ_u. Because the compatibility is enforced between elements, the adopted model is defined as a displacement formulation. Let us express the approximations as:

$$\begin{aligned}\mathbf{u} &= \mathbf{U}_v\mathbf{q} \quad \text{in } V,\\ \mathbf{t} &= \mathbf{T}\mathbf{p} \quad \text{on } \Gamma_u,\end{aligned} \tag{12}$$

where matrix $\mathbf{U}_v$ collects the approximation functions of the displacements in the domain and the matrix $\mathbf{T}$ corresponds to the approximations of the tractions on the boundary Γ_u of each finite element. The vectors $\mathbf{q}$ and $\mathbf{p}$ list the associated weights.

Imposing that the dual variables in the discrete and continuum models produce the same work, it is possible to define the generalized body forces in the domain, $\mathbf{Q}_v$, and the generalized displacements on the kinematic boundary, $\mathbf{v}$:

$$\begin{aligned}\mathbf{Q}_v &= \int \mathbf{U}_v^t\mathbf{b}\,\mathrm{d}V,\\ \mathbf{v} &= \int \mathbf{T}^t\bar{\mathbf{u}}\,\mathrm{d}\Gamma_u.\end{aligned} \tag{13}$$

The equilibrium equation in the domain of each finite element and the compatibility equation on the kinematic boundary Γ_u are enforced on average as follows:

$$\int \mathbf{U}_v^t(\mathbf{D}\boldsymbol{\sigma} + \mathbf{b})\,\mathrm{d}V = \mathbf{0}, \tag{14}$$

$$\int \mathbf{T}^t(\mathbf{u} - \bar{\mathbf{u}})\,\mathrm{d}\Gamma_u = \mathbf{0}. \tag{15}$$

Using the definition of the generalized variable $\mathbf{Q}_v$ (Eq. (13)) in Eq. (14) and integrating by parts, one obtains:

$$-\int (\mathbf{D}^*\mathbf{U}_v)^t\boldsymbol{\sigma}\,\mathrm{d}V + \int (\mathbf{N}^*\mathbf{U}_v)^t\boldsymbol{\sigma}\,\mathrm{d}\Gamma_u + \int (\mathbf{N}^*\mathbf{U}_v)^t\boldsymbol{\sigma}\,\mathrm{d}\Gamma_\sigma = -\mathbf{Q}_v, \tag{16}$$

where the matrix $\mathbf{N}\{\mathbf{N}^*\}$ contains the components of the unit outward normal vector to the static boundary Γ_σ associated with $\mathbf{D}\{\mathbf{D}^*\}$.

The final equilibrium equation of the discrete model is obtained by introducing in the previous expression the constitutive relation, the compatibility equation in the domain, the equilibrium equation on the boundary and the approximation defined in Eq. (12):

$$\widetilde{\mathbb{K}}\mathbf{q} - \mathbf{B}\mathbf{p} = \mathbf{Q}_v + \mathbf{Q}_\Gamma \quad \text{in } V, \tag{17}$$

where:

$$\widetilde{\mathbb{K}} = \int (\mathbf{D}^*\mathbf{U}_v)^t\,\widetilde{\mathbf{K}}\,(\mathbf{D}^*\mathbf{U}_v)\,\mathrm{d}V, \tag{18}$$

$$\widetilde{\mathbf{K}} = (1-d)\,\mathbf{E}, \tag{19}$$

$$\mathbf{B} = \int \mathbf{U}_v^t\mathbf{T}\,\mathrm{d}\Gamma_u, \tag{20}$$

$$\mathbf{Q}_\Gamma = \int \mathbf{U}_v^t\mathbf{t}_\gamma\,\mathrm{d}\Gamma_\sigma. \tag{21}$$

Including the approximations (12) in Eq. (15), one can obtain the compatibility equation on the kinematic boundary Γ_u for the discrete model:

$$-\mathbf{B}^t\mathbf{q} = -\mathbf{v} \quad \text{on } \Gamma_u. \tag{22}$$

Combining Eqs. (17) and (22), we obtain the following solving system for each finite element:

$$\begin{bmatrix} \widetilde{\mathbb{K}} & -\mathbf{B} \\ -\mathbf{B}^t & \mathbf{0} \end{bmatrix} \begin{Bmatrix} \mathbf{q} \\ \mathbf{p} \end{Bmatrix} = \begin{Bmatrix} \mathbf{Q}_v + \mathbf{Q}_\Gamma \\ -\mathbf{v} \end{Bmatrix}. \tag{23}$$

The global governing system is assembled by direct allocation of the contribution of each elementary system. The continuity between finite elements is assured only by the operator **B** since all the others matrices of the governing system are independent for each finite element.

4. Implementation of the hybrid-displacement models

This section presents the three variants for the hybrid-displacement formulation considered in this paper.

4.1. Hybrid(-Trefftz) displacement formulation

In the first model adopted in this work, the domain approximation functions are derived from the bi-harmonic stress potential equation governing 2D elastostatic problems for homogeneous, isotropic and linear elastic material, expressed in polar coordinates (Timoshenko and Goodier, 1970; Cismaşiu, 2000):

$$\left(\frac{\partial^2}{\partial r^2}+\frac{1}{r}\frac{\partial}{\partial r}+\frac{1}{r^2}\frac{\partial^2}{\partial \theta^2}\right)\left(\frac{\partial^2 \Phi}{\partial r^2}+\frac{1}{r}\frac{\partial \Phi}{\partial r}+\frac{1}{r^2}\frac{\partial^2 \Phi}{\partial \theta^2}\right)=0. \tag{24}$$

To define the approximation for the boundary tractions complete sets of Chebyshev polynomials defined over a master edge $\xi \in [-1.0, 1.0]$ are used:

$$T = \cos(n \cos^{-1} \xi). \tag{25}$$

In linear elasticity, the model corresponds to a hybrid-Trefftz displacement formulation. When damage starts to develop, the finite element model degenerates into a hybrid-displacement formulation, because the material is no longer homogeneous and so the Navier equation is no longer verified *a priori*. The approximation basis of the linear elastic regime works then as a general approximation basis, loosing part of the advantages of the approximation functions chosen. The model is therefore called a hybrid(-Trefftz) formulation instead of a hybrid-Trefftz displacement formulation or hybrid-displacement formulation.

The approximation functions for the displacements are rather complicated, so the approximations in this model are usually written in the form:

$$\begin{aligned} &\mathbf{u} = \mathbf{U}_{v1}\mathbf{q}_1 + \mathbf{U}_{v2}\mathbf{q}_2 \quad \text{in } V, \\ &\mathbf{t} = \mathbf{T}\mathbf{p} \quad \text{on } \Gamma_u, \end{aligned} \tag{26}$$

where matrix $\mathbf{U}_{v1}$ collects the approximation functions of the strain-inducing displacements in the domain, matrix $\mathbf{U}_{v2}$ defines the rigid-body modes and matrix **T** corresponds to the approximations of the tractions on the boundary Γ_u. The vectors $\mathbf{q}_1, \mathbf{q}_2$ and **p** list the associated weights.

For two-dimensional analysis, if the domain approximation is linear, three independent approximation functions are obtained in $\mathbf{U}_{v1}$. Then, an increase of one degree in the approximation leads to the enrichment of the basis $\mathbf{U}_{v1}$ with four new independent functions, as explained in Freitas et al. (1999b).

Proceeding as described in Section 3, we obtain the following governing system for each finite element (Cismaşiu, 2000):

$$\begin{bmatrix} \widetilde{\mathbb{K}}_1 & \mathbf{0} & -\mathbf{B}_1 \\ \mathbf{0} & \mathbf{0} & -\mathbf{B}_2 \\ -\mathbf{B}_1^t & -\mathbf{B}_2^t & \mathbf{0} \end{bmatrix} \begin{Bmatrix} \mathbf{q}_1 \\ \mathbf{q}_2 \\ \mathbf{p} \end{Bmatrix} = \begin{Bmatrix} \mathbf{Q}_{v1} + \mathbf{Q}_{\Gamma 1} \\ \mathbf{Q}_{v2} + \mathbf{Q}_{\Gamma 2} \\ -\mathbf{v} \end{Bmatrix}, \tag{27}$$

with

$$\begin{cases} \widetilde{\mathbb{K}}_i = \int (\mathbf{D}^* \mathbf{U}_{vi})^t \widetilde{\mathbf{K}} (\mathbf{D}^* \mathbf{U}_{vi}) \, dV \\ \mathbf{B}_i = \int \mathbf{U}_{vi}^t \mathbf{T} \, d\Gamma_u \\ \mathbf{Q}_{\Gamma i} = \int \mathbf{U}_{vi}^t \mathbf{t}_\gamma \, d\Gamma_\sigma \\ \mathbf{Q}_{vi} = \int \mathbf{U}_{vi}^t \mathbf{b} \, dV \qquad (i = 1, 2) \end{cases}. \tag{28}$$

Denoting by n_u the number of generalized displacements $\mathbf{q} = \mathbf{q}_1 + \mathbf{q}_2$ and n_p the number of generalized tractions **p**, the kinematic indeterminacy $\beta = n_u - n_p$ should be non-negative to avoid inconsistency in the compatibility conditions and as small as possible to ensure a strong T-residual enforcement of the inter-element displacement continuity conditions (Cismaşiu, 2000).

Because the approximation functions are filtered in order to verify the Navier equation in the linear elastic regime, the formulation is associated to few degrees of freedom (dof) and the solution of the symmetric nonlinear system (27) requires low computational effort. Due to the nonlinear behavior of the material, it is necessary to use an iterative procedure to obtain the correct matrix $\widetilde{\mathbf{K}}_1$. All the other matrices present in the governing system are computed only once.

4.2. Hybrid(-Trefftz) displacement formulation enriched with Heaviside functions

In a nonlocal damage model the degradation of the material is represented by a jump in the displacement field along a narrow band, the fracture process zone. The strain distribution along this band is highly localized but remains continuous. Because the approximation functions are *filtered* in order to verify the Trefftz condition, the hybrid(-Trefftz) displacement formulation does not model correctly this type of behavior, as is demonstrated in Sections 5 and 6. For this reason, a second model is tested. It corresponds to a hybrid(-Trefftz) displacement formulation enriched with Heaviside functions. This local *p*-refinement gives *a priori* knowledge about the character of the problem and its solution. The Heaviside functions chosen are inspired in the work of Patzák and Jirásek (2003), who use these type of functions in the context of the extended finite elements.

The ideal situation would be to introduce a local function changing with the evolution of damage, in order to simulate the evolution of the displacement and strain fields. This type of function is very difficult to define and would be associated to a high computational effort. For this reason, Patzák and Jirásek suggest the use of several Heaviside functions, each one representing a certain stage of damage in the material, and consequently associated with a certain profile for the displacement and strain fields. These functions should allow the correct representation of the evolution of the strain and displacement fields in the direction perpendicular to the crack. The adopted Heaviside functions have the following expression in a one-dimensional case:

$$H(r, A_j) = \begin{cases} 0 & \text{if } r < -A_j \\ \frac{315}{256 A_j} \int_{-A_j}^{r} \left(1 - \frac{\xi^2}{A_j^2}\right)^4 d\xi & \text{if } |r| < A_j \\ 1 & \text{if } r > A_j \end{cases}. \tag{29}$$

The scaling $315/(256A_j)$ allows the control of the interaction radius and leads to value one for $H(r, A_j)$ when $r = A_j$. The variable r represents the distance of a certain point P to the center of the process zone, P_{ZPF}, so $r = \sqrt{(P - P_{ZPF})^2}$.

The definition of functions $H(r, A_j)$ is inspired in the behavior of an uniaxial tension test. Fig. 1(a) represents the function $H(r, A_j)$ for different values of A_j. Depending on the value of the parameter A_j, the functions $H(r, A_j)$ approximate a smoother or sharper jump. As expected, the derivative of function $H(r, A_j)$ has a profile similar to a localized strain field in a nonlocal damage model, see Fig. 1(b).

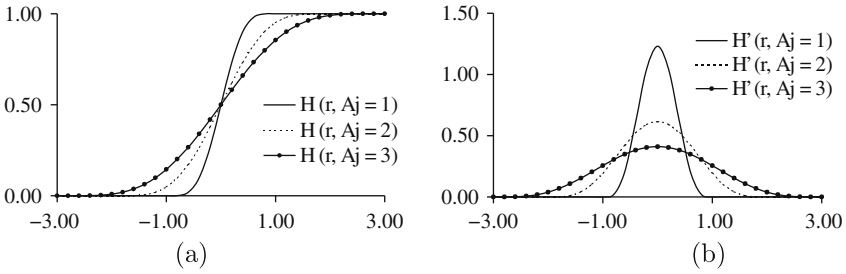

Fig. 1. Heaviside functions and their derivatives for different values of parameter A_j.

According to Patzák and Jirásek (2003), by selecting different values for the parameter A_j, one can construct a series of enrichment functions describing the evolving profile in the direction perpendicular to the crack, which allows the association of the material's behavior with the Heaviside functions. It is assumed that the parameter A_j depends on the maximum value of the damage variable installed in the material, d_j, in a way that the Heaviside function (29) approximates the nonlocal characteristic length in a one-dimensional problem, λ_c, obtained, for example, with a wave propagation analysis. For this reason, each Heaviside function with opening $2 \times A_j$ may be associated with a damage value d_j and a nonlocal characteristic length of λ_{c_j}.

In a 2D analysis, the properties of the Heaviside functions should be carefully chosen. The real behavior suggests 2D Heaviside functions that evolve both in the directions perpendicular and parallel to the crack, since the crack is usually not developed in the whole structure. However, a numerical analysis with these type of functions would be very complex and computationally too demanding. If one adopts a 2D Heaviside function constant in the direction of the crack, as represented in Fig. 2, it is possible to approximate the localized solution for certain geometries. Since the numerical performance of the hybrid(-Trefftz) displacement formulation enriched with the Heaviside function is validated using the numerical examples presented in Fig. 10, in which damage quickly propagates to the section around the notch, a 2D Heaviside function as the one represented in Fig. 2 is suitable for the analysis. As illustrated in Section 6, the proposed formulation enriched with local functions presents some drawbacks. Therefore, no further effort has been made to generalize the proceeding for a more complex problem.

Since we use hybrid finite elements, the independent Heaviside functions may be added directly to the approximation basis (local p-refinement). The new approximations are expressed as:

$$\mathbf{U}_{v1}\,\mathbf{q}_1 = \mathbf{U}_{v1_T}\,\mathbf{q}_{v_T} + \mathbf{U}_{v1_L}\,\mathbf{q}_{v_L}, \tag{30}$$

where matrix $\mathbf{U}_{v1_T}$ collects the Trefftz functions and matrix $\mathbf{U}_{v1_L}$ is defined by the local Heaviside approximation functions. The corresponding weights are $\mathbf{q}_{v_T}$ and $\mathbf{q}_{v_L}$.

In order to simplify the presentation of the implementation details, we assume in the following text that only one Heaviside function is added to the approximation basis. Two different approaches are available. In the first one, we add the Heaviside function independently to the approximation basis defined for each finite element. A second possibility corresponds to define the Heaviside function globally, in the sense that its weight is the same for all the finite elements in which the Heaviside function is considered. In the first approach, the total number of degrees of freedom is increased by the number of finite elements in which the Heaviside function is considered. In the second case, it increases only by one. The work presented here adopts the second approach.

Using a two finite element mesh and one Heaviside function, the global governing system may be written in the form (31). The subscripts T and H symbolize the type of functions used for the computation of the operators, T stands for Trefftz functions and H stands for Heaviside function.

$$\begin{bmatrix}
\mathbb{K}^{\text{elem1}}_{1_{TT}} & \mathbf{0} & & & \mathbb{K}^{\text{elem1}}_{1_{TH}} & -\mathbf{B}^{\text{elem1}}_{1_T} \\
\mathbf{0} & \mathbf{0} & & & & -\mathbf{B}^{\text{elem1}}_{2} \\
 & & \mathbb{K}^{\text{elem2}}_{1_{TT}} & \mathbf{0} & \mathbb{K}^{\text{elem2}}_{1_{TH}} & -\mathbf{B}^{\text{elem2}}_{1_T} \\
 & & \mathbf{0} & \mathbf{0} & & -\mathbf{B}^{\text{elem2}}_{2} \\
(\mathbb{K}^{\text{elem1}}_{1_{TH}})^t & & (\mathbb{K}^{\text{elem2}}_{1_{TH}})^t & & (\mathbb{K}^{\text{elem1}}_{1_{HH}} + \mathbb{K}^{\text{elem2}}_{1_{HH}}) & -(\mathbf{B}^{\text{elem1}}_{1_H} + \mathbf{B}^{\text{elem2}}_{1_H}) \\
-\mathbf{B}^{\text{elem1}^t}_{1_T} & -\mathbf{B}^{\text{elem1}^t}_{2} & -\mathbf{B}^{\text{elem2}^t}_{1_T} & -\mathbf{B}^{\text{elem2}^t}_{2} & -(\mathbf{B}^{\text{elem2}}_{1_H} + \mathbf{B}^{\text{elem2}}_{1_H})^t & \mathbf{0}
\end{bmatrix}. \tag{31}$$

4.3. Hybrid-displacement formulation with orthogonal Legendre polynomials

In this hybrid-displacement formulation, all approximations are defined as linear combinations of complete sets of orthogonal Legendre polynomials defined over a master element ($\xi, \eta \in [-1.0, 1.0]$).

Each line in the approximation matrices corresponds to a block of Legendre polynomials used to define the approximation of a given independent generalized variable. Let us use the displacement component u_x as an example: following (Pereira and Freitas, 2000), we define $u_x = \Sigma P_i(\xi) \times P_j(\eta) \times q^{ij}$, where $P_i(\xi)\{P_j(\eta)\}$ corresponds to the Legendre polynomial of degree $i\{j\}$ in direction $\xi\{\eta\}$ and q^{ij} is the associated weight. The use of these polynomials leads to highly sparse solving systems and allows the construction of analytical expressions for the computation of most of the operators

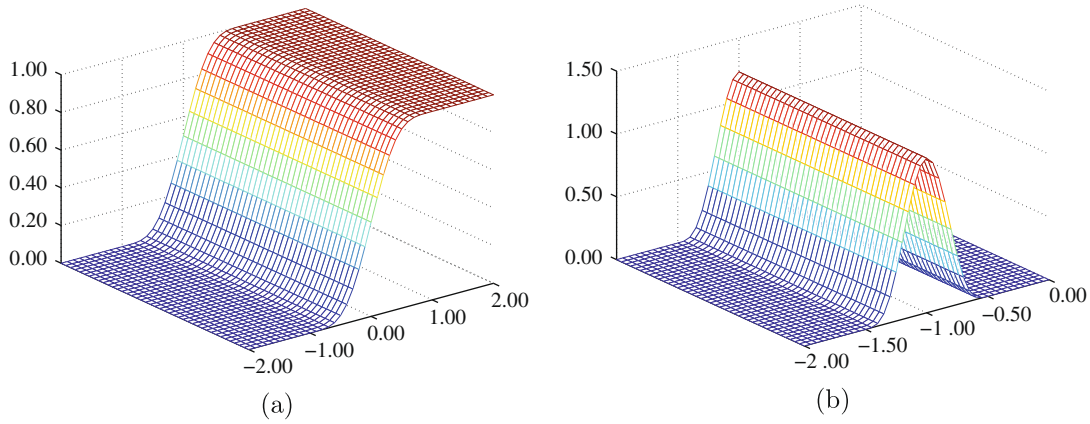

Fig. 2. (a) Heaviside function for 2D analysis and (b) its derivative.

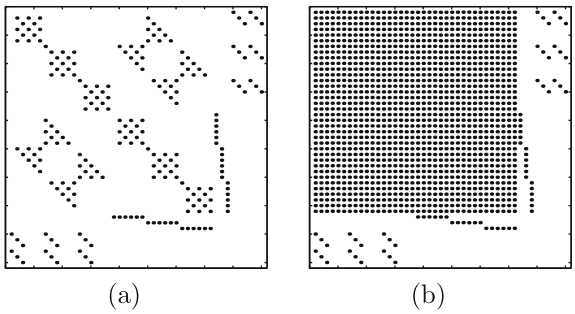

Fig. 3. Nonzero coefficients in an elementary governing system assuming a (a) linear and (b) nonlinear behavior for the material.

(Pereira and Freitas, 2000) present in the governing system. In fact, only the matrix $\widetilde{\mathbb{K}}$ requires the use of numerical integration schemes.

While the behavior is linear elastic, the governing system is very sparse, see Fig. 3(a). When this behavior ceases to be verified, most of the coefficients in the generalized elementary stiffness matrix $\widetilde{\mathbb{K}}$ are nonzero. By analyzing Fig. 3(b), one may conclude that any p-refinement of the displacement approximation basis will increase the number of nonzero coefficients. Consequently, it can become computationally very expensive to solve the nonlinear system in the form (23). In order to optimize the numerical performance of the hybrid-displacement formulation, three different implementations are considered:

(1) Implementation (I1) solves the governing system in the form (23);
(2) Implementation (I2) assumes a constant generalized stiffness matrix $\mathbb{K}$ and introduces an additional vector on the right hand side of the governing system, $\boldsymbol{\sigma}_0$, as follows:

$$\boldsymbol{\sigma} = \widetilde{\mathbf{K}}\boldsymbol{\varepsilon} = \mathbf{E}\boldsymbol{\varepsilon} + \boldsymbol{\sigma}_0. \tag{32}$$

The equilibrium equation in the discrete model is then written in the format:

$$\mathbb{K}\mathbf{q} - \mathbf{B}\mathbf{p} = \mathbf{Q}_v + \mathbf{Q}_\Gamma + \overline{\mathbf{Q}} \quad \text{in } \mathbf{V}, \tag{33}$$

where:

$$\mathbb{K} = \int (\mathbf{D}^*\mathbf{U}_v)^t\,\mathbf{E}\,(\mathbf{D}^*\mathbf{U}_v)\,\mathrm{d}V; \quad \overline{\mathbf{Q}} = \int (\mathbf{D}^*\mathbf{U}_\mathbf{v})^\mathbf{t}\,\mathbf{E}\,\boldsymbol{\varepsilon}\mathbf{d}\,\mathrm{d}\mathbf{V}. \tag{34}$$

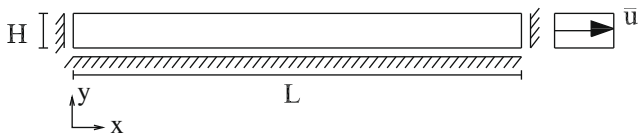

Fig. 4. Uniaxial tension test.

(3) Implementation (I3) is similar to (I2) but assumes an update of the operator $\widetilde{\mathbb{K}}$ in the first iteration of the load step (n) whenever the number of iterations of load step $(n-1)$ is higher than a certain fixed value. The equilibrium equation in the discrete model in this case is:

$$\widetilde{\mathbb{K}}_n^0\mathbf{q} - \mathbf{B}\mathbf{p} = \mathbf{Q}_v + \mathbf{Q}_\Gamma + \overline{\mathbf{Q}}_* \quad \text{in } \mathbf{V}, \tag{35}$$

with:

$$\widetilde{\mathbb{K}}_n^0 = \int (\mathbf{D}^*\mathbf{U}_v)^t\,\mathbf{E}\,(1-d_n^0)\,(\mathbf{D}^*\mathbf{U}_v)\,\mathrm{d}V, \tag{36}$$

$$\overline{\mathbf{Q}}_* = \int (\mathbf{D}^*\mathbf{U}_v)^t\,\mathbf{E}\,\boldsymbol{\varepsilon}(d-d_n^0)\,\mathrm{d}V. \tag{37}$$

5. Tension test

Consider the structure presented in Fig. 4, subjected to a prescribed displacement loading programme. This example is used to validate the hybrid(-Trefftz) and the hybrid displacement models being discussed and to compare their relative performance. To trigger the damage localization, the axial stiffness at the left boundary has been slightly weakened.

It is assumed that $L = 100$ mm and $H = 20$. The concrete's behavior is approximated assuming the damage model described in

Table 1
Tension test: discretizations adopted for the analysis with the hybrid(-Trefftz) displacement formulation.

Test	1	2	3	4	5
No. of elements	1	1	1	1	4
$\mathbf{U}_v$	8	10	15	18	4
$\mathbf{T}$	7	10	10	15	2
Gauss/elem.	(20×20)	(20×20)	(20×20)	(25×25)	(5×5)
N_{dof}	58	75	95	122	108

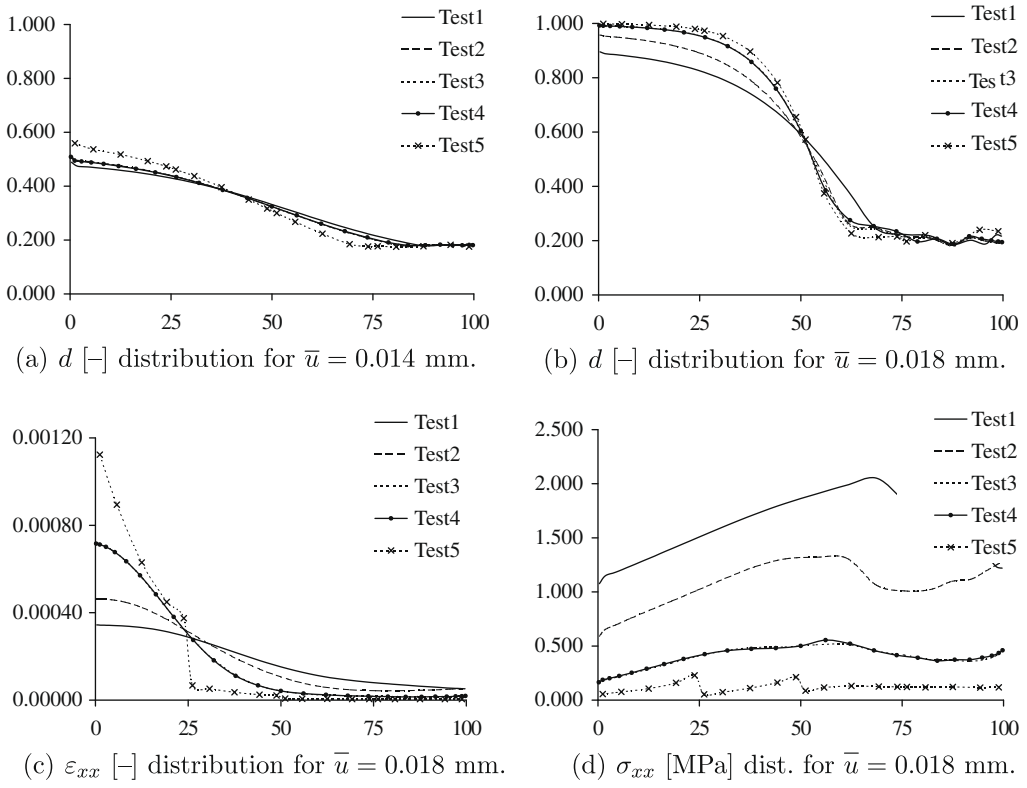

Fig. 5. Tension test: *p*-refinement and *h*-refinement.

Section 3 with the following characteristics: $n = 2, k = 0.00015$ MPa, $c = 2.72, l = 20$ mm and $E = 30$ GPa, $\upsilon = 0.00$.

Since the Poisson coefficient is assumed to be zero, the behavior of the plate in tension is analogous to the behavior of a bar in an uniaxial tension test. Nevertheless, a bidimensional analysis is chosen in order to test the performance of the Trefftz functions adopted in the hybrid(-Trefftz) displacement formulation. In a one-dimensional problem these approximation functions are simplified and it is not possible to identify some of the properties associated to the proposed model. Since the problem is 2D, the integration points mesh is also defined in two dimensions. The Gauss quadrature rule is adopted.

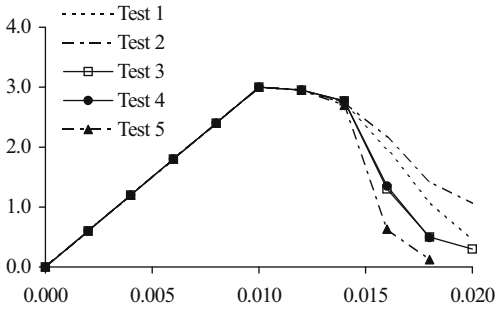

Fig. 6. Tension test: global response.

5.1. Hybrid(-Trefftz) displacement formulation

For the analysis of the plate presented in Fig. 4 two regular finite element meshes are considered with one and four elements, respectively. Table 1 lists the characteristics of the approximations for the different tests performed. It presents the degree of approximation for the displacement fields in the domain, $\mathbf{U}_v$ and the degree of the approximation defined for the tractions on the kinematic boundary, $\mathbf{T}$. The same table presents also the number of Gauss points considered in each element and the total number of degrees of freedom associated with each discretization, N_{dof}.

The approximation basis and the mesh must be sufficiently rich to allow for a correct reproduction of the damage evolution. Fig. 5 compares the results obtained with a set of discretizations corresponding to different *p*- and *h*-refinement.

Tests 1 and 2 cannot reproduce correctly nor the damage nor the strain distribution along the bar for $u = 0.018$ mm, because the degree of the approximation is not high enough. In terms of stress distribution, these two tests show unacceptable residual values. Introducing a *p*-refinement, Tests 3 and 4, it is possible to notice a significant improvement in the quality of the results. No major improvement is obtained from Test 3 to Test 4, which suggests that the solution provided by these discretizations is accurate.

One would expect that an *h*-refinement would lead to the same localized solution. However, the results obtained with Test 5 show

Table 2
Tension test: numerical tests of the hybrid-displacement formulation with orthogonal Legendre polynomials.

Test	1	2	3	4
No. of elements	1	1	1	2
$\mathbf{U}_v^s$	15	10	5	4
$\mathbf{U}_v^n$	4	4	4	4
$\mathbf{T}$	3	3	3	3
Gauss/elem.	(20×5)	(20×5)	(20×5)	(10×5)
N_{dof}	172	122	72	120

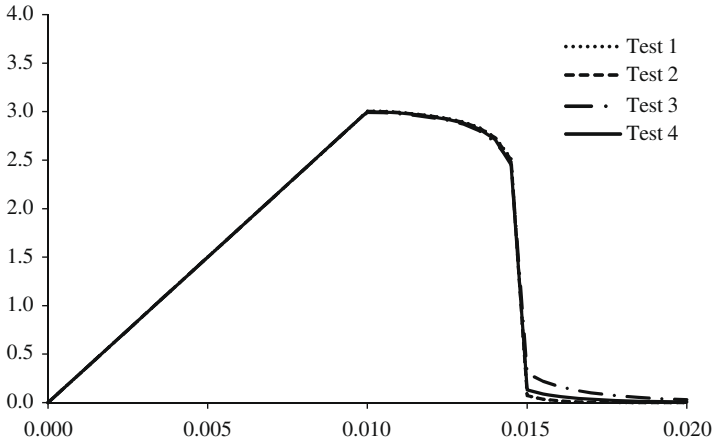

Fig. 7. Tension test: global response with the hybrid-displacement model.

a different pattern for ε_{xx} and σ_{xx} when $\bar{u} = 0.018$ mm. On one hand, the strain distribution presents a discontinuity between finite elements and a higher peak value for ε_{xx}. On the other hand, the stress distribution obtained with Test 5 shows an almost complete dissipation of stresses.

In truth, the hybrid-displacement formulation presented in Section 3 does not impose the continuity of the strain field between finite elements. Nevertheless, one would expect that a *p*-refinement or an *h*-refinement would minimize the discontinuities between elements, but the numerical results contradict this expectation. One possible explanation to justify this type of behavior is the fact that the approximation basis used to model the displacement field is not complete, due to the filter imposed by the use of the Trefftz condition. This aspect will be discussed in detail in the second example.

Fig. 6 presents the global response of the structure in terms of load–displacement curve. All test cases using the mesh with one element do not reproduce correctly the global softening behavior. However, the load–displacement curves obtained using the single element mesh and higher degrees of the approximation are closer to the curve obtained with Test 5, as expected. When the degree of the approximation in the domain is not

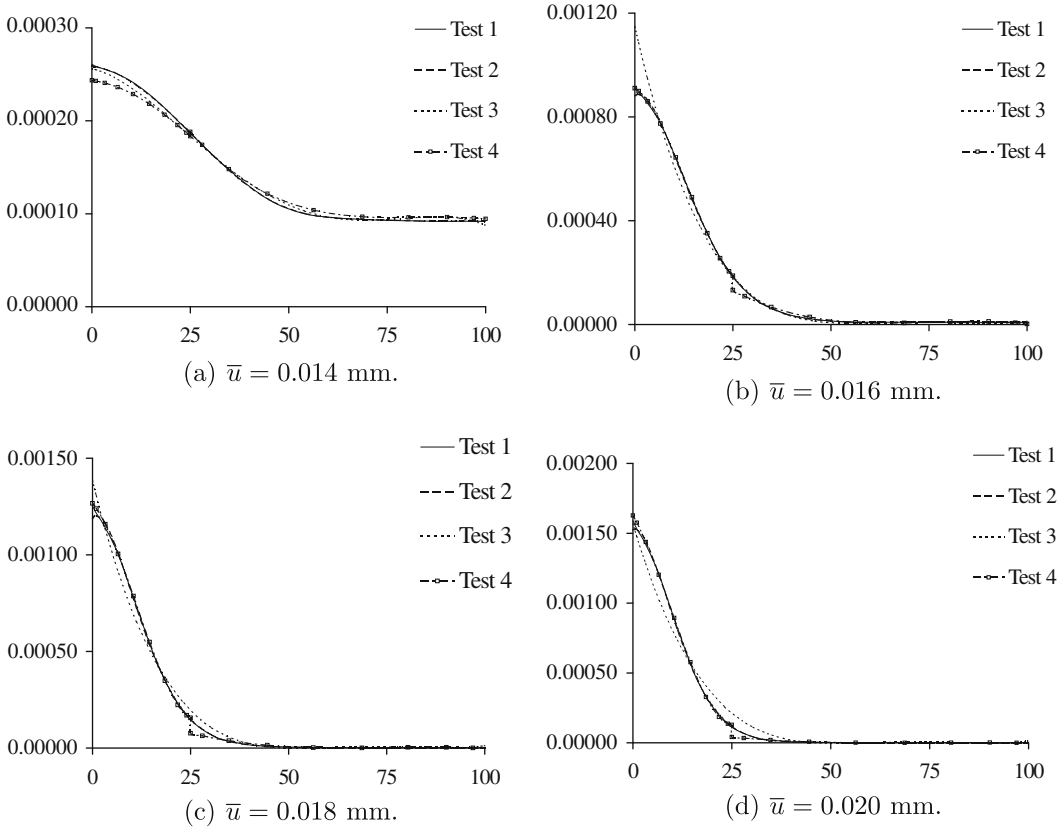

Fig. 8. Tension test: ε_{xx} [–] strain field evolution for all test cases.

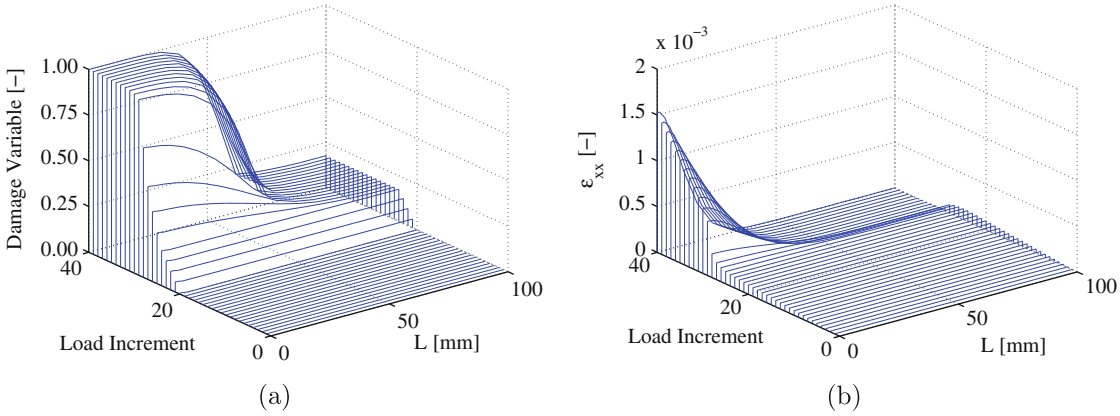

Fig. 9. Tension test: evolution of (a) damage distribution (b) ε_{xx} [–] strain field.

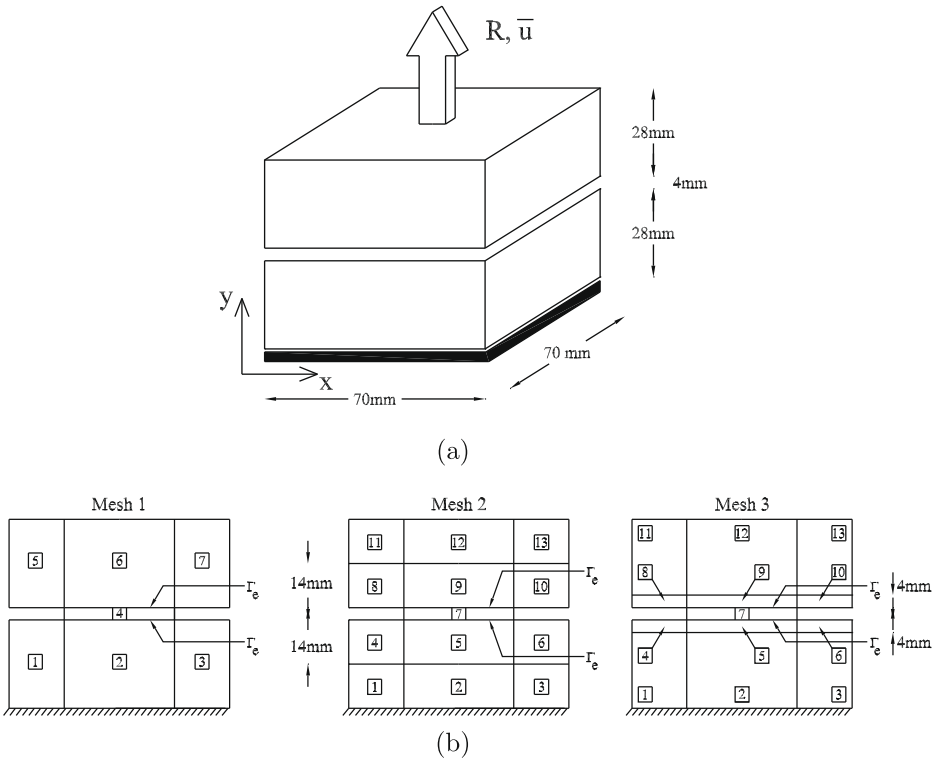

Fig. 10. Hassanzadeh test: (a) Definition of the problem and (b) finite element meshes.

enough, the model localizes in a larger bandwidth, i.e., a smaller part of the structure unloads due to the load increment. Therefore, the solutions obtained with insufficient degrees of approximation in the domain dissipate less energy due to unloading and their load–displacement curve is "above" the correct solution.

5.2. Hybrid-displacement formulation with orthogonal Legendre polynomials

The same structure is now analyzed using the hybrid-displacement formulation based on the use of Legendre polynomials. Two regular meshes, with one and two elements are taken into consideration.

Table 2 summarizes the characteristics of the discretizations considered in this analysis. For each test case, it is assumed that

Table 3
Hassanzadeh test: discretizations with the hybrid(-Trefftz) model.

Test	1	2	3	4
Mesh	1	2	3	1
$\mathbf{U}_v$	10 (elem. 2, 6) 8 (elem. 4) and 5 (others)	8 (elem. 5, 7, 9) 6 (elem. 2, 12) and 5 (others)	8 (elem. 5, 7, 9) 6 (elem. 2, 12) and 5 (others)	20 (elem. 2, 4, 6) and 15 (others)
$\mathbf{T}$	7 front. Γ_e[a] and 3 others	7 front. Γ_e[a] and 2 others	7 front. Γ_e[a] and 2 others	15 front. Γ_e[a] and 10 others
Lobatto/ elem.	(15×15)	(15×15)	(15×15)	(20×20)
N_{dof}	318	482	482	778

[a] As indicated in Fig. 10.

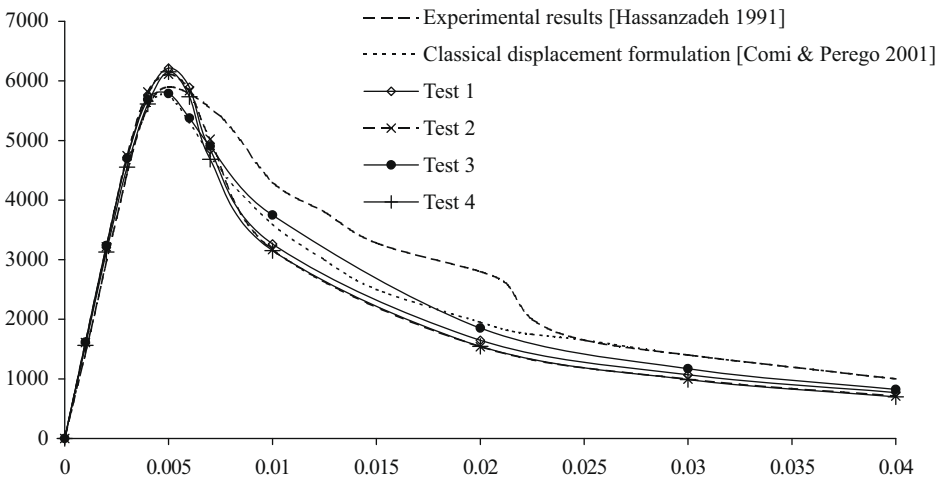

Fig. 11. Hassanzadeh test: load R [N]- prescribed displacement $\bar{u}$ [mm] diagrams obtained with the hybrid(-Trefftz) model.

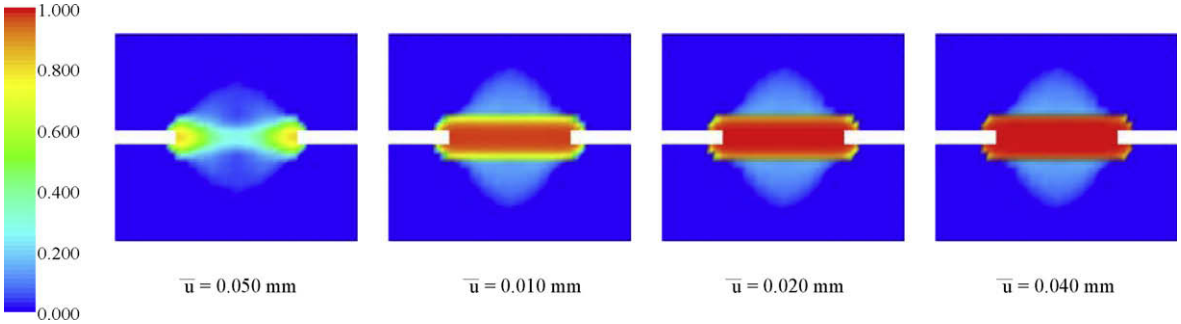

Fig. 12. Hassanzadeh test: damage evolution with Test 1.

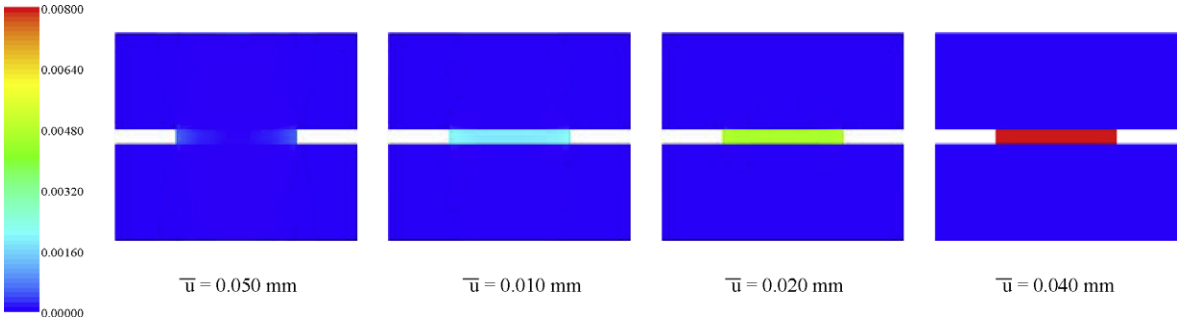

Fig. 13. Hassanzadeh test: ε_{yy} [–] strain distribution with Test 1.

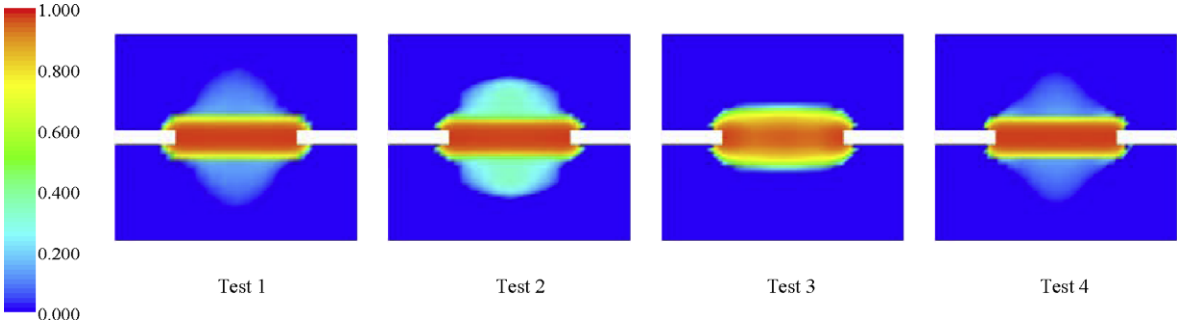

Fig. 14. Hassanzadeh test: damage distribution [–] when $\bar{u} = 0.010$ mm.

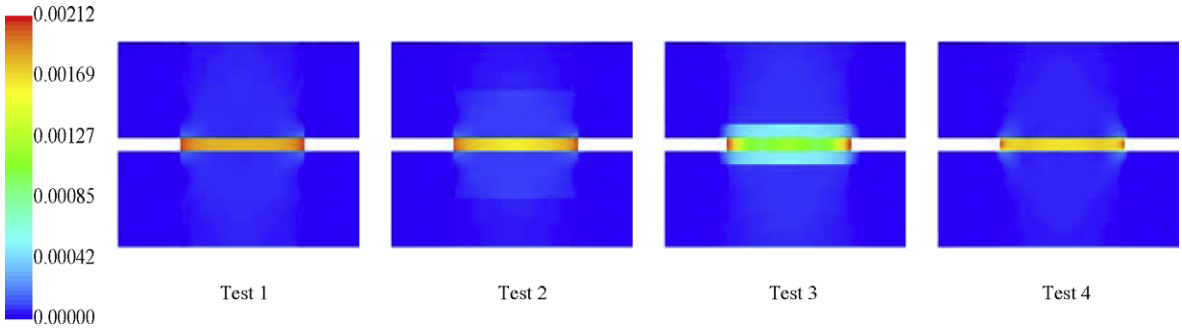

Fig. 15. Hassanzadeh test: ε_{yy} [–] strain distribution when $\bar{u} = 0.010$.

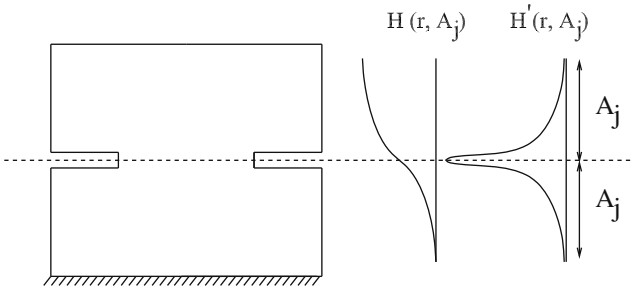

Fig. 16. Hassanzadeh test: definition of local functions.

Table 4
Hassanzadeh test: evolution for the absolute value of the weight $\mathbf{q}_{v_L}$ when $A_j = 10$ mm.

$\bar{u}$[mm]	0.005	0.010	0.020	0.030	0.035	0.040
$\mathbf{q}_{v_L}$	0.98	6.72	13.34	16.04	16.61	16.84

the degree of the approximation **T** is the same for all kinematic boundaries.

The load–displacement curves obtained with all hybrid-displacement discretizations show an objective response, as illustrated in Fig. 7. When comparing the plots presented in this figure and Fig. 6, one may verify that only an *h*-refinement of the hybrid(-Trefftz) approximation correctly models the objective global response.

The evolution of the strain profile obtained with the four discretizations is presented in Fig. 8. It can be observed that as strain localization evolves, the approximation provided by Test 3 is not sufficiently rich to model correctly the strain profile. But, contrarily to what happens with the hybrid(-Trefftz) formulation, the hybrid-displacement model based on the use of Legendre polynomials ensures the convergence to an objective response, using either a *p*- or an *h*-refinement procedure.

In this model, the continuity of the strain field between finite elements is not imposed. However, since the displacement approximation basis is now complete, any type of refinement of the approximation leads to a coherent solution and the discontinuities observed in the strain profile tends to be neglectful.

Fig. 9 represents the evolution of the damage d and the strain field ε_{xx} distributions along the axis of the plate obtained with Test 2. The evolution of the process zone is correctly modeled. In fact, the localization within the bar, i.e., unloading in some elements, occurs for $\lambda_{cr} < 200$ mm. Using Eq. (11) with $\lambda_{cr} = 200$ mm and $l = 20$ mm, we obtain a value for damage in the unloading zone of $d \simeq 0.20$, which is in good agreement with the value observed in that zone in Fig. 9(a). Unloading is easily identified by the strain distribution along the bar. Please notice that it is possible to have an increase in the damage variable in a certain cross section while unloading occurs because the model is nonlocal. For high values of damage, $\frac{\lambda_{cr}}{2\pi l}$ reaches values around 0.80, so $\lambda_{cr} \simeq 100$ mm, corresponding to a width for the

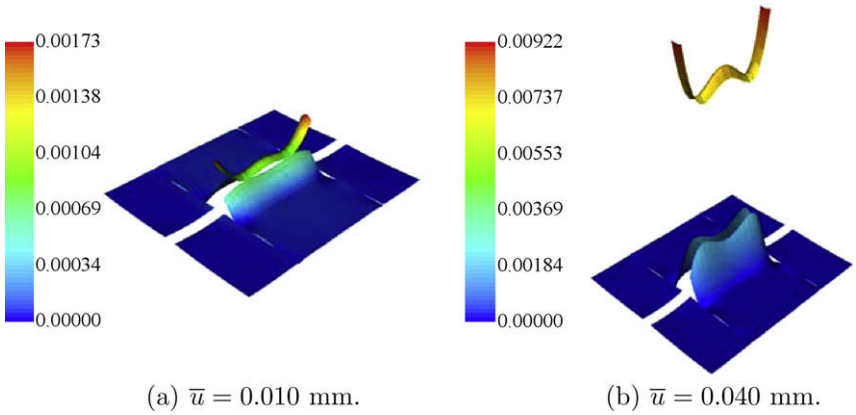

Fig. 17. Hassanzadeh test: ε_{yy} [–] strain field evolution in Test 1.

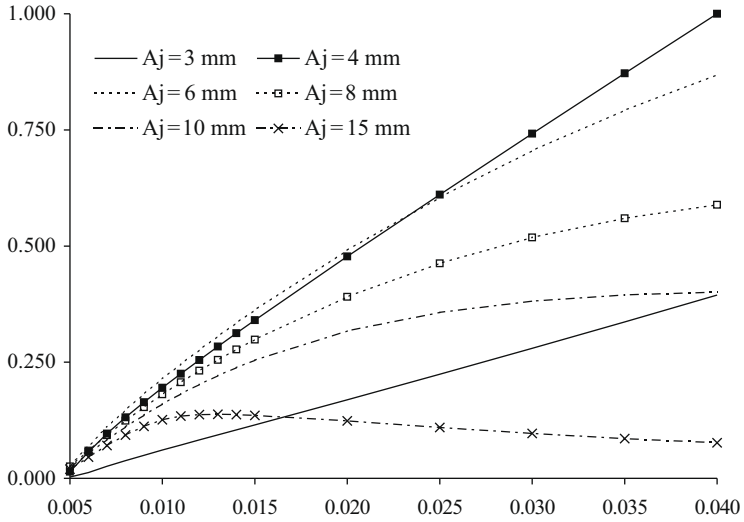

Fig. 18. Hassanzadeh test: normalized $\mathbf{q}_{v_L}$ evolution for different values of parameter A_j.

localization zone in the bar of about 50 mm. This value is also directly recovered from Fig. 9(a).

6. Hassanzadeh's test

This example corresponds to the numerical simulation of the experimental tension test performed by Hassanzadeh (1991) on a four edge notched concrete specimen with dimensions $(70 \times 70 \times 60)$ mm, see Fig. 10(a). The lower edge is fixed and the normal displacement of the upper edge is controlled. The test produces only damage in tension, so the adopted constitutive model is suitable for the analysis. This example has been modeled by several authors (Comi and Perego, 2000, 2001b; diPrisco et al., 2000).

In Comi and Perego (2001b), the authors Comi and Perego adopt a classical displacement formulation and the damage model described in Section 3. As the constitutive model is the same, the results obtained with the hybrid-displacement formulations are compared with the numerical results presented (Comi and Perego, 2001b) and also with the experimental results given in Hassanzadeh (1991). This test illustrates the performance of the hybrid(-Trefftz) displacement formulation and the enrichment of the corresponding approximation basis with local Heaviside functions. It also shows the potential associated with hybrid-displacement models based on the use of orthogonal Legendre polynomials.

Following the work of Comi and Perego (2001b), we assume the following material parameters: $n = 12$, $k = 5.8 \times 10^{-14}$ MPa, $c = 405$, $l = 1.6$ mm, $E = 36$ GPa and $\upsilon = 0.15$. Although the problem exhibits a three-dimensional behavior due to the notch geometry, a plane strain condition is assumed in the numerical model. To account for the three-dimensionality of the real problem, the total vertical reaction is obtained by weighing the reaction at the upper edge with the area of influence of the real problem (Comi, 2001).

The three finite element meshes shown in Fig. 10(b) are chosen to study the discontinuities of the strain field between finite elements.

6.1. Hybrid(-Trefftz) displacement formulation

Table 3 summarizes the characteristics of the discretizations used in the numerical tests performed with the hybrid(-Trefftz) displacement formulation.

Fig. 11 compares the global load R–displacement $\bar{u}$ curve for the four tests. All discretizations model the global behavior with satisfactory accuracy but only Test 3 approximates the reaction R peak value with the same precision as the classical displacement formulation presented in (Comi and Perego, 2001b).

The evolution for the damage distribution obtained with Test 1 is shown in Fig. 12. As expected, damage starts to develop at the notches and then expands defining an almost horizontal major crack. However, damage expands to regions where the behavior of the material should remain linear elastic. Fig. 13 shows the ε_{yy} strain field distribution. For small prescribed displacement values, ε_{yy} is almost continuous between elements. For larger prescribed displacement values, the strain field discontinuity tends to increase and at the final stage of the loading procedure the strain is concentrated only at element 4.

Figs. 14 and 15 present the damage and the ε_{yy} strain component distributions obtained with the different discretizations for a prescribed displacement value given by $\bar{u} = 0.010$ mm. In Tests 1, 2 and 4 one may observe damage beyond the region of the notch. These values are not expected and are not visible in the results provided by Test 3.

In terms of the ε_{yy} strain component distribution, important discontinuities are noticeable between finite elements when the discretizations 1, 2 or 4 are chosen. Due to the finite element mesh adopted in Test 3, the discontinuities in the strain field are minimized.

The discretization associated with Test 4 can be viewed as a p-refinement of discretization 1. An uniform h-refinement applied to discretization 1 may lead to the discretization adopted in Test 2. Both these refinements slightly improve the quality of the ε_{yy} strain component distribution for small values of the imposed displacement, but do not avoid the concentration of the strain evolution around the notch for higher values of the prescribed displacement. As pointed out before, this behavior is due to the use of the Trefftz condition in the definition of the approximation bases. According to this condition, the approximation functions are required to satisfy all field equations in the domain of the structure. The functions used in the models being tested are generated assuming a linear elastic behavior for the material. When damage appears, the constitutive relations are no longer linear and the approximation functions do not define a complete set. As the approximation basis is not

complete, no *p*-refinement will improve the performance of the model and only a localized *h*-refinement close to the fracture process zone improves the strain distribution diagram. This is visible not only in the damage and strain distributions but also in the curve R–$\bar{u}$ obtained for the different test cases.

6.2. Hybrid(-Trefftz) displacement formulation enriched with heaviside functions

To improve the performance of the hybrid(-Trefftz) displacement models and to minimize the development of strain discontinuities between elements localized inside the process fracture zone, let us enrich the approximation basis by including a set of local Heaviside functions.

As the direction of the crack is known in advance for the Hassanzadeh Test, the definition of the local enrichment functions is straightforward, as illustrated in Fig. 16. The *opening* of each function is given by $2 \times A_j$. The value for this parameter can be optimized taking into consideration the prediction of the nonlocal characteristic length, λ_{c_j}, associated to a given value of damage, d, through the use of Eq. (11). For $d_j = 0.50 \Rightarrow \lambda_{c_j} \approx 20$ mm $\Rightarrow A_j = 10$ mm and $d_j \to 1.00 \Rightarrow \lambda_{c_j} \approx 8.0$ mm $\Rightarrow A_j = 4$ mm.

To study the influence of the value assigned to parameter A_j, several test cases are taken into consideration. All of these cases use the discretization associated with the Test 1 presented in Table 3. To ensure the accuracy of the numerical integrations and the behavior of the nonlocal model when considering local functions, a Lobatto quadrature rule considering 20×20 points per element

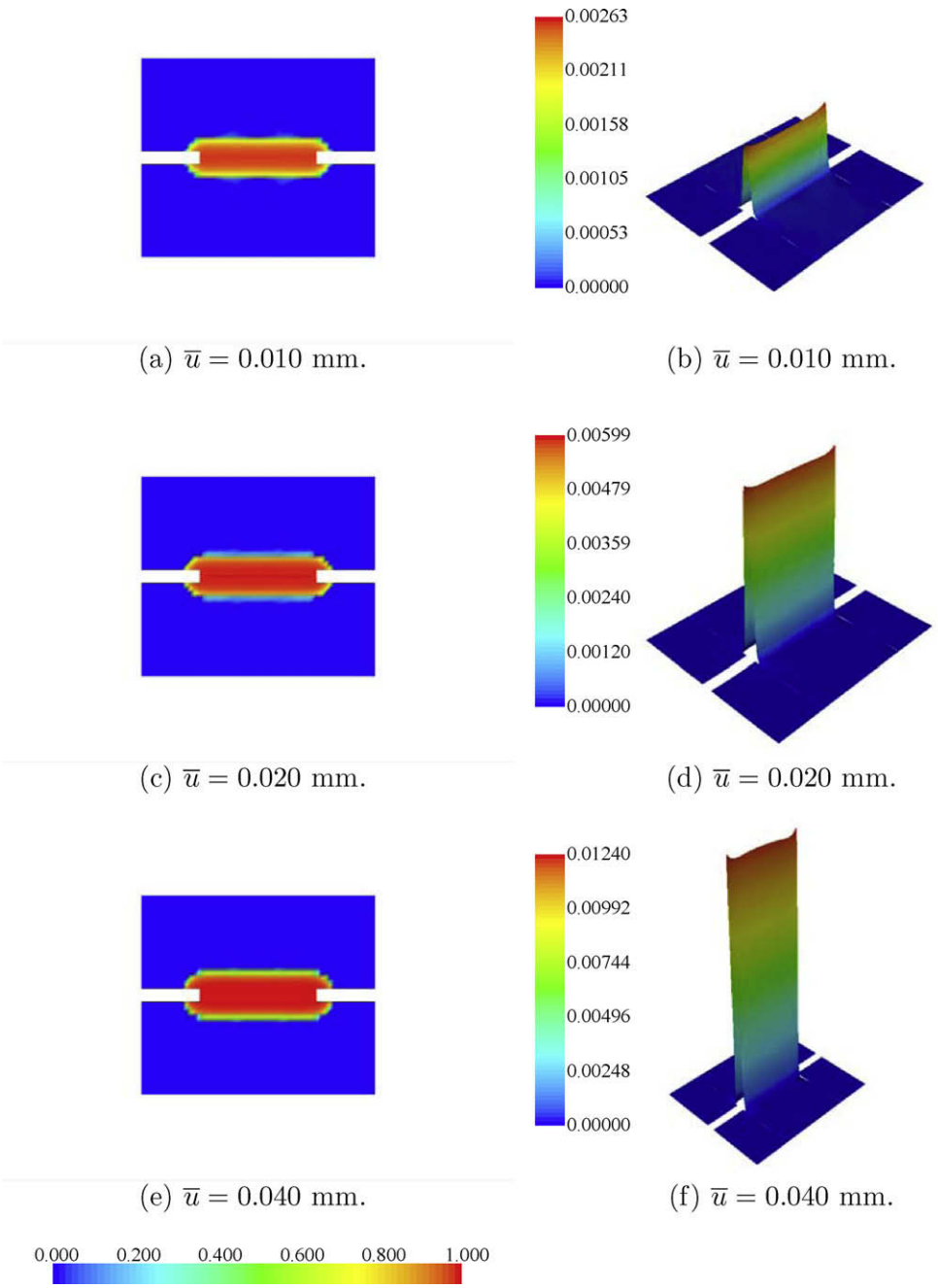

Fig. 19. Hassanzadeh test: damage [–] distribution [–] (left) and ε_{yy} [–] strain field (right) with $A_j = 4$ mm.

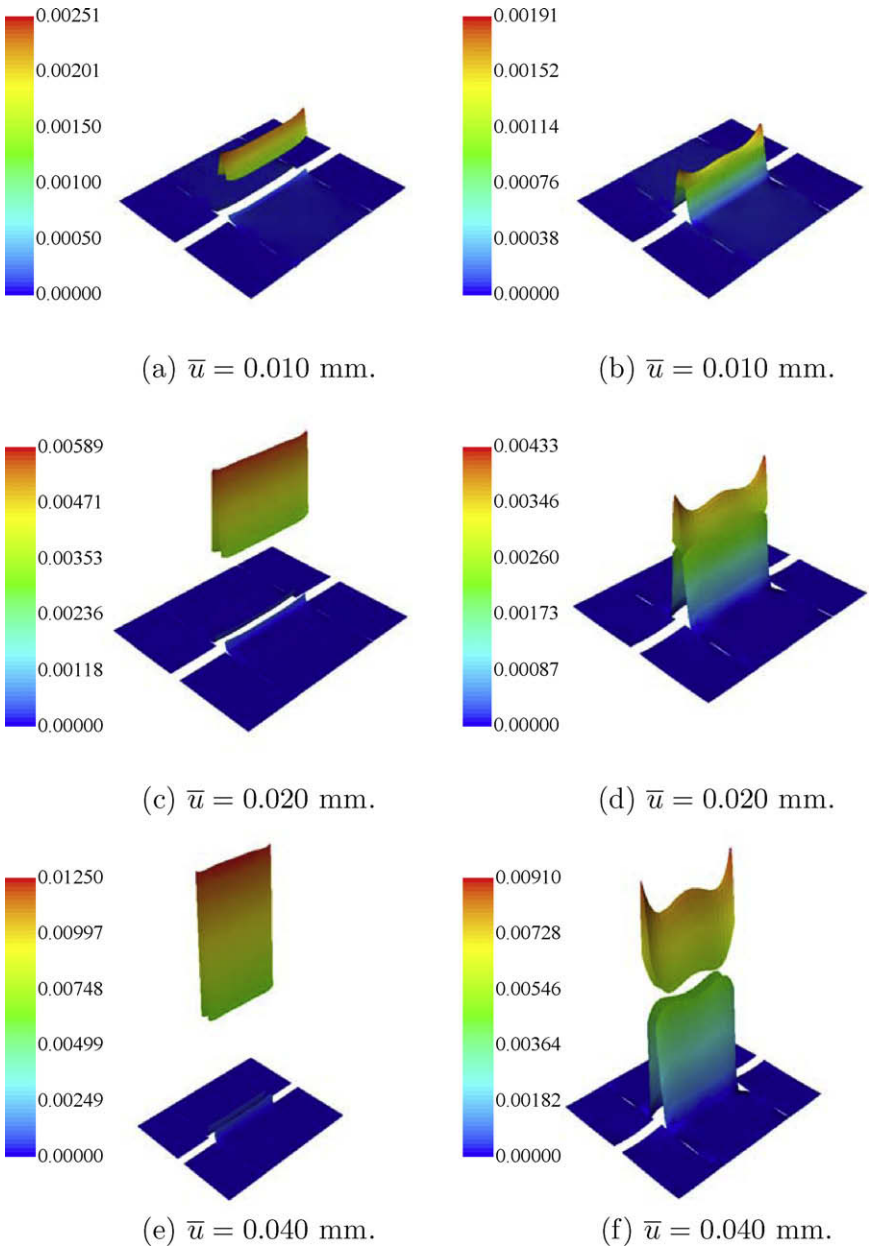

Fig. 20. Hassanzadeh test: ε_{yy} [–] strain field evolution with $A_j = 3$ mm (left) and $A_j = 6$ mm (right).

Table 5
Hassanzadeh test: discretizations tested with hybrid displacement formulations.

Test	1	2	3
$\mathbf{U}_v^{\xi}$	6	6 (elem. 2, 4, 6) and 4 (others)	9 (elem. 2, 4, 6) and 4 (others)
$\mathbf{U}_v^{\eta}$	9 (elem. 2, 4, 6) and 6 (others)	9 (elem. 2, 4, 6) and 4 (others)	9 (elem. 2, 4, 6) and 4 (others)
$\mathbf{T}^{\xi,\eta}$	5	3 except $\mathbf{T}^{\eta}_{\text{elem4}} = 8$	3 except $\mathbf{T}^{\eta}_{\text{elem4}} = 8$
N_{dof}	956	726	906
CPU[c] [s]	6824(I3)[a] and 152755(I1)[b]	– –	9586(I3)[a]

[a] As defined in Section 4.3 and adopting 50 as the maximum number of iterations in each load increment.
[b] As defined in Section 4.3.
[c] In a Pentium 4, 2996 MHz machine.

is used. Elements 2, 4, and 6 in Fig. 10(b) are enriched with the local function.

Lets us consider $A_j = 10$ mm. Table 4 lists the absolute value of the weight associated with the local function, $\mathbf{q}_{v_L}$, for different values of the prescribed displacement. It can be observed that the influence of this function is not important for values of the prescribed displacement larger than $\bar{u} = 0.030$ mm. This is an expected result, since $A_j = 10$ mm is adequate for damage values around $d = 0.5$ and not for advanced stages of the loading procedure.

Fig. 17 reinforces this idea by representing the ε_{yy} strain field for two different values of the prescribed displacement. For $\bar{u} = 0.040$ mm there is a clear discontinuity in the strain field between elements, and the results are quite similar to those obtained with the hybrid(-Trefftz) displacement model without local functions.

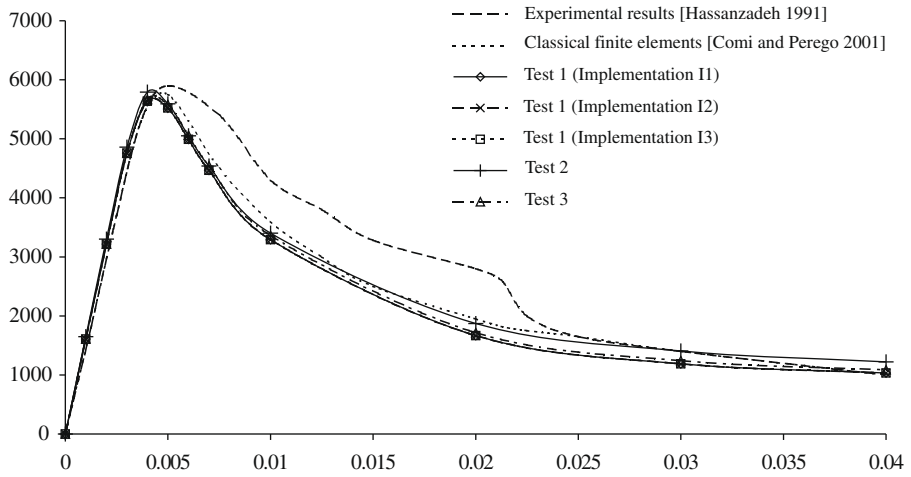

Fig. 21. Hassanzadeh test: load R [N] – prescribed displacement $\bar{u}$ [mm] diagrams.

Fig. 18 presents the normalized weight $\mathbf{q}_{v_L}$ (in absolute value) obtained for different parameters A_j and for all the stages of the loading process and leads to the conclusion that the best value for the opening parameter is $A_j = 4$ mm.

This may be confirmed by the analysis of Fig. 19, where the damage and ε_{yy} strain distributions obtained considering a local function with $A_j = 4$ mm are presented for different prescribed displacement values. It is possible to verify that the strain field continuity between elements is now ensured. In fact, the continuity of the strain field is not imposed. However, the continuity of the displacement filed is imposed on average in a weighted-residual form. If the model is working properly, an *h*-refinement or *p*-refinement should minimize the discontinuities of the displacement field and, consequently, of the strain field.

According to Fig. 18, with a different choice for the value of parameter A_j, the influence of the local Heaviside function is smaller. Consequently, the effectiveness of the correction induced by this function tends to get smaller also. This is illustrated in Fig. 20, where the ε_{yy} strain field evolution is presented for the test cases with $A_j = 3$ mm and $A_j = 6$ mm. In these cases the discontinuities between elements appear again. As suggested by the analysis of Fig. 18, these discontinuities are less important for $A_j = 6$ mm than for $A_j = 3$ mm.

The test cases presented before clearly show that the correct choice for parameter A_j is an important issue when local Heaviside functions are used to enrich the hybrid(-Trefftz) approximation. To solve this problem one could include in the approximation basis several local functions with different values of A_j. Then, the numerical model should be able to *select* the appropriate function to activate at different stages of the loading process. However, this procedure leads to highly ill-conditioned governing systems and the final results may be strongly affected by this fact. This is an opened issue that has to be investigated in future research work.

A second difficulty associated with the use of a local function is the identification of the direction of the major crack. In the example discussed here this is not a problem due to the geometry of the structure, but in a more general case this identification and the definition of a correct local function is not so straightforward.

6.3. Hybrid-displacement formulation with orthogonal Legendre polynomials

The use of hybrid-displacement formulations based on orthogonal Legendre polynomials is now illustrated. Table 5 shows the characteristics of the three discretizations tested. Only the seven element mesh is adopted. The approximation is defined to be richer at the elements 2,4 and 6 and three different degrees for the approximation along direction x are considered. As expected, the use of a hybrid-displacement model leads to larger number of degrees of freedom when compared to the hybrid(-Trefftz) displacement model.

Fig. 21 presents the load–displacement diagrams obtained with the three test cases. The solutions are compared with experimental data and with the numerical results obtained by Comi and Perego (2001b). It is important to verify that all test cases give similar results, so the expected regularization is achieved and the objectivity is ensured. The lack of positive hardening, also present in Comi and Perego (2001b), leads to a more brittle behavior in the softening branch for both numerical techniques. The bump experimentally observed in the softening branch is due to rotational instability (Comi and Perego, 2001b) and therefore is not present in the numerical simulations.

Table 5 shows that the use of implementation (I1) leads to unacceptable CPU times, due mainly to the high computational cost associated with the governing system updating at each iteration. This conclusion is reinforced in Fig. 22, where the CPU time required to set-up and to solve the governing system and the number of iterations required in each step of the loading process are plotted for the three implementations under discussion. It is clear that implementation (I1) is associated always with high CPU times, especially when the nonlinear process starts. On the other hand, the use of implementation (I2) is associated with an increasing number of iterations per load step. This number of iterations becomes unacceptable as softening evolves. Implementation (I3) corresponds to the best compromise between the CPU time required and the efficiency of the iterative procedure. Whenever implementation (I3) is used, it is assumed that 50 is the maximum number of iterations in each load increment.

Fig. 23 presents the damage distribution, the u_y displacement field and the ε_{yy} strain component distribution obtained with Test1 for an advanced stage and for the final stage of the loading process. The solution is quite accurate. Nevertheless, some discontinuities in the u_y displacement field between elements are observed. These discontinuities are due to an unexpected behavior of ε_{yy} along direction x, as shown in Fig. 23(f).

The u_y discontinuities associated with Test 1 can be minimized by increasing the degree for the tractions approximation on the kinematic boundaries, in particular by increasing the maximum

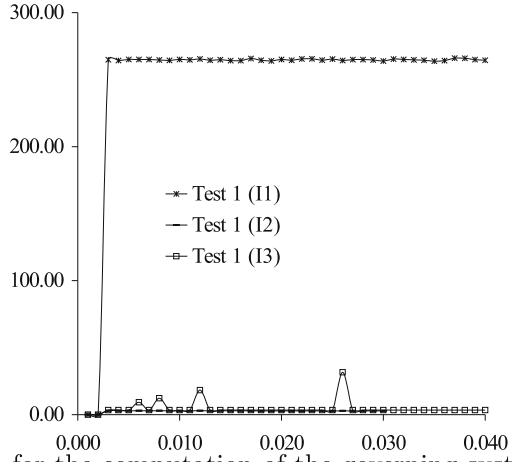

(a) CPU time for the computation of the governing system [seconds].

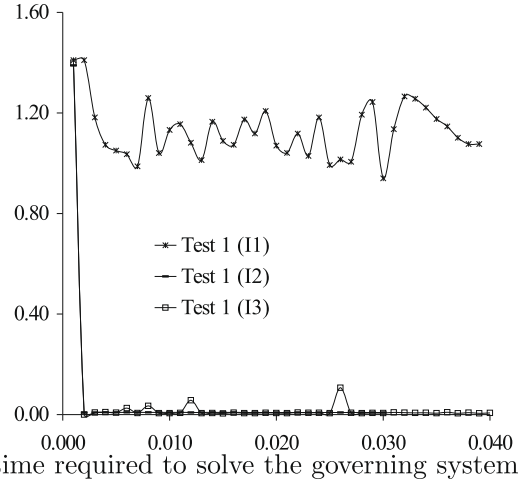

(b) CPU time required to solve the governing system [seconds].

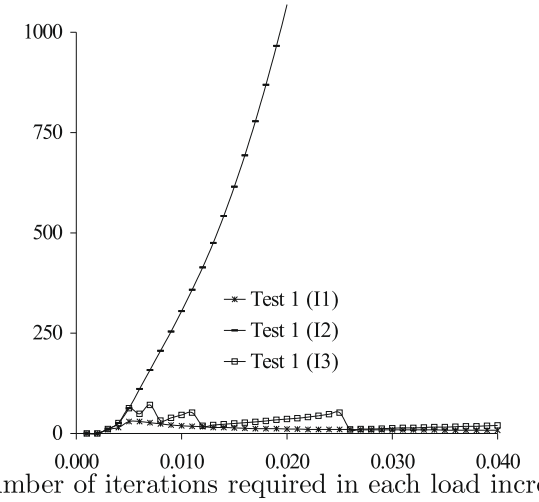

(c) Number of iterations required in each load increment.

Fig. 22. Hassanzadeh test: numerical performance for the alternative implementations.

degree in $\mathbf{T}''_{\text{elem4}}$. This effect is illustrated in Fig. 24, where the results obtained with Test 3 are presented. The u_y displacement field is now continuous and accurate representation for the ε_{yy} strain distribution is achieved.

Finally, Fig. 25 presents the damage evolution, represented in the deformed shape of the structure.

7. Conclusions

This paper presents and discusses three different hybrid-displacement finite element models combined with a nonlocal isotropic damage model for the analysis of structures with softening materials.

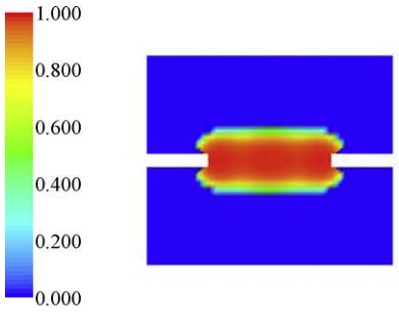

(a) Damage [–] for $\overline{u} = 0.020$ mm.

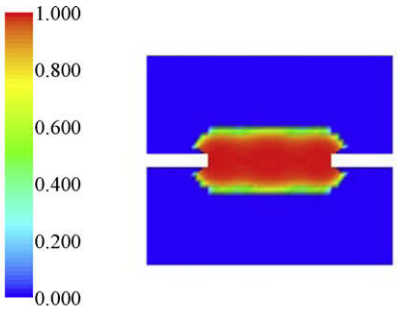

(b) Damage [–] for $\overline{u} = 0.040$ mm.

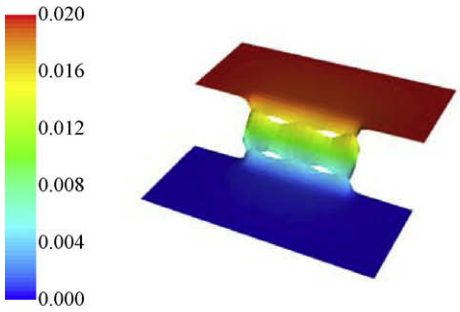

(c) u_y [mm] for $\overline{u} = 0.020$ mm.

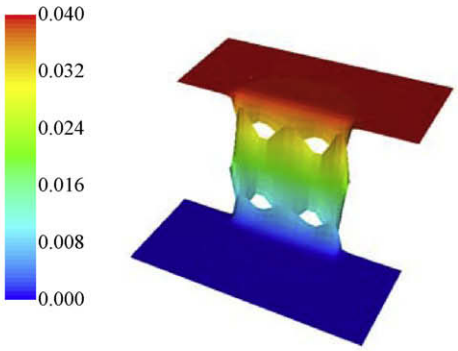

(d) u_y [mm] for $\overline{u} = 0.040$ mm.

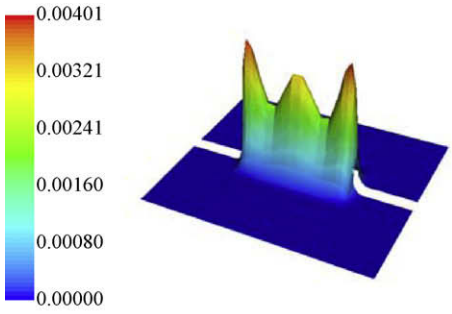

(e) ε_{yy} [–] for $\overline{u} = 0.020$ mm.

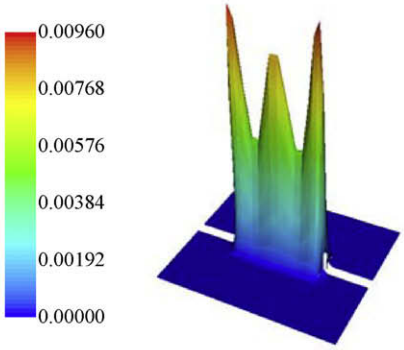

(f) ε_{yy} [–] for $\overline{u} = 0.040$ mm.

Fig. 23. Hassanzadeh test: solutions obtained with Test 1.

The hybrid(-Trefftz) displacement formulation has the main advantage of using a set of functions satisfying all domain equations in the zone where the material presents a linear elastic behavior. However, in the zones where damage evolves, the approximation functions do not define a complete set and consequently cannot correctly reproduce the response of the structure. The numerical results show that the global behavior is recovered but some inconsistencies are obtained, namely in the strain field and damage distribution.

To overcome the drawbacks associated with the use of the hybrid(-Trefftz) formulation, a second model is implemented an tested. It is based on the definition of a hybrid(-Trefftz) basis enriched with local Heaviside functions defined on the process fracture zone. A correct choice for parameter A_j, which defines the *opening* of that local function, will lead to accurate solutions. However, two main issues set this approach aside: how to construct the local basis when the location and direction of the crack is not known *a priori* and how to select the appropriate value for parameter A_j for a general situation.

The hybrid-displacement model based on the use of orthogonal Legendre polynomials overcomes most of the drawbacks presented by the two other models, in spite of requiring always a larger number of degrees of freedom. To ensure the numerical efficiency of this model, the implementation (I3) described in Section 4.3 should be used. Otherwise, the model can be computationally too demanding in terms of CPU time required by the analysis.

An interesting approach for future research corresponds to the combination of the hybrid(-Trefftz) formulation and the hybrid-displacement model based on Legendre polynomials. The first type

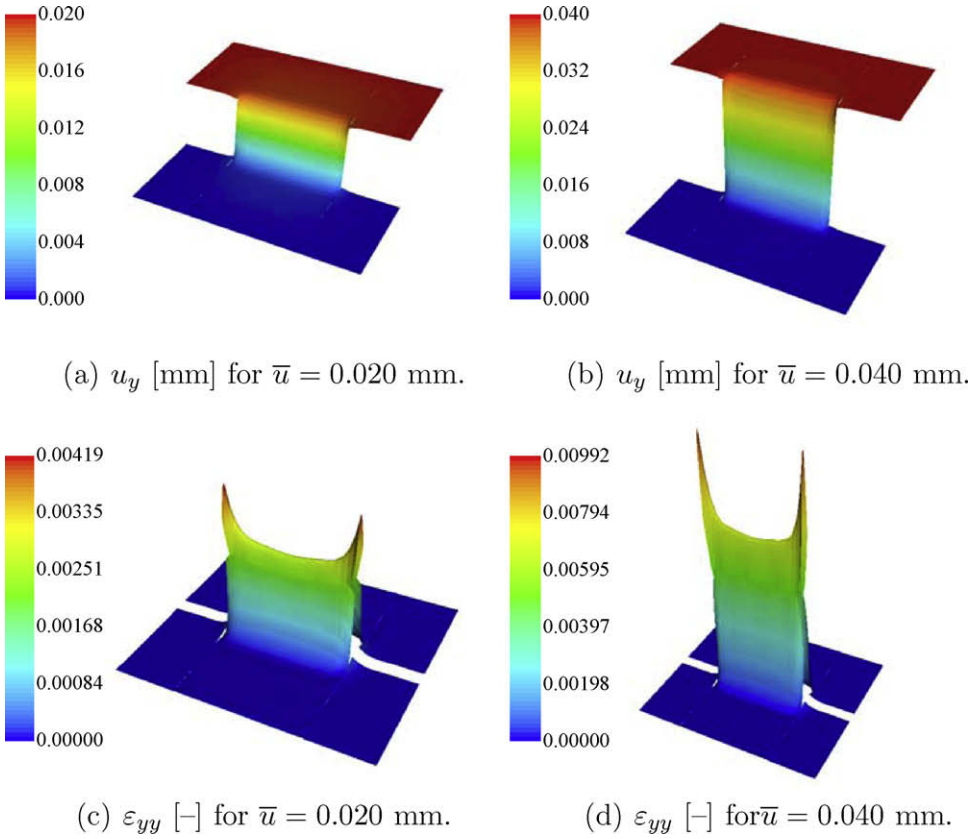

(a) u_y [mm] for $\overline{u} = 0.020$ mm. (b) u_y [mm] for $\overline{u} = 0.040$ mm.

(c) ε_{yy} [–] for $\overline{u} = 0.020$ mm. (d) ε_{yy} [–] for$\overline{u} = 0.040$ mm.

Fig. 24. Hassanzadeh Test: solutions obtained with Test 3.

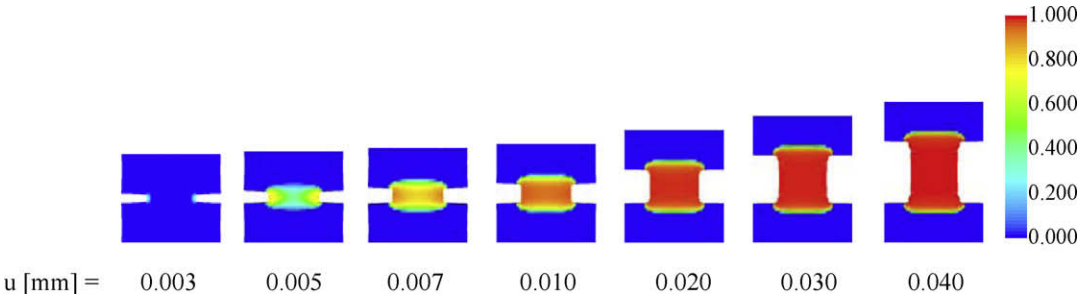

Fig. 25. Hassanzadeh test: damage distribution evolution in Test 3.

of approximation should be used where the material presents a linear elastic behavior, and the hybrid-displacement Legendre approximation should be implemented only at the regions where damage is expected to evolve.

Another promising field of investigation is the combined use of a Trefftz model with a discrete constitutive model. A local Heaviside-like function will be used to approximate the crack and a hybrid-Trefftz formulation models the rest of the domain, where a linear elastic behavior is installed so the potentialities of the Trefftz formulation are valid.

Acknowledgements

This work has been partly supported by "Fundação para a Ciência e a Tecnologia" through projects "Financiamento Plurianual", POCTI/ECM/33066/2001 and the Ph.D. scholarship SFRH/BD/9050/2002.

References

Bažant, Z.P., 1976. Instability, ductility, and size effect in strain-softening concrete. ASCE Journal of Engineering Mechanics 102, 331–344.
Bažant, Z.P., Jirásek, M., 2002. Nonlocal integral formulations of plasticity and damage: survey of progress. ASCE Journal of Engineering Mechanics 128, 1119–1149.
Bažant, Z.P., Pijaudier-Cabot, G., 1989. Measurement of characteristic length of nonlocal continuum. ASCE Journal of Engineering Mechanics 115, 755–767.
Castro, L.M.S.S., 1996. Wavelets e séries de Walsh em elementos finitos. PhD thesis, Instituto Superior Técnico, Universidade Técnica de Lisboa, Lisboa.
Cismaşiu, C., 2000. The hybrid-Trefftz displacement element for static and dynamic structural analysis problems. PhD thesis, Instituto Superior Técnico, Universidade Técnica de Lisboa, Lisboa.
Comi, C., 1999. Computational modelling of gradient-enhanced damage in quasi-brittle materials. Mechanics of Cohesive-frictional Materials 4, 17–36.
Comi, C., 2001. A non-local model with tension and compression damage mechanics. European Journal of Mechanics A/Solids 20, 1–22.
Comi, C., Perego, U., 2000. A bi-dissipative damage model for concrete with applications to dam engineering. In: Proceedings of the European Congress on Computational Methods and Applied Sciences and Engineering, ECCOMAS 2000, Barcelona.

Comi, C., Perego, U., 2001a. Fracture energy based bi-dissipative damage model for concrete. International Journal of Solids and Structures 38, 6427–6454.
Comi, C., Perego, U., 2001b. Nonlocal aspects of nonlocal damage analyses of concrete structures. European Journal of Finite Elements 10, 227–242.
Comi, C., Perego, U., 2001c. Symmetric and non-symmetric non-local damage formulations: an assessment of merits. In: Proceedings of the European Conference on Computational Methods, ECCM-2001, Cracow.
di Prisco, M., Ferrara, L.F., Meftah, J.P., de Borst, R., Mazars, J., Reynouard, J.M., 2000. Mixed mode fracture in plain and reinforced concrete: some results on benchmark tests. International Journal of Fracture 103, 127–148.
Freitas, J.A.T., Almeida, J.P.M., Pereira, E.M.B.R., 1999a. Non-conventional formulations for the finite element method. Computational Mechanics 23, 488–501.
Freitas, J.A.T., Cismaşiu, C., Wang, Z.M., 1999b. Comparative analysis of hybrid-Trefftz stress and displacements elements. Archives of Computational Mechanics Engineering 6, 1–26.
Hassanzadeh, M., 1991. Behaviour of fracture process zone in concrete influenced by simultaneous applied normal and shear displacements. Ph.D. thesis, Lund Institute of Technology, Lund.
Jirásek, M., 2001. Modelling of localized damage and fracture in quasibrittle materials. In: Vermeer, P.A. et al. (Eds.), Continuous and Discontinuous Modelling of Cohesive Frictional Materials, Lecture Notes in Physics, vol. 568. Springer, Berlin, pp. 17–29.
LaBorderie, C., 1991. Phenomenes unilateraux dans un materiau endommageable: modelisation et application a l'analyse de structures en beton. PhD thesis, Université Paris 6, Paris.
Lemaitre, J., 1992. A Course on Damage Mechanics, first ed. Springer-Verlag.
Mazars, J., Pijaudier-Cabot, G., 1989. Continuum damage theory – application to concrete. ASCE Journal of Engineering Mechanics 115, 345–365.
Patzák, B., Jirásek, M., 2003. Process zone resolution by extended finite elements. Engineering Fracture Mechanics 70, 957–977.
Peerlings, R.H.J., de Borst, R., Brekelmans, W.A.M., de Vree, J.H.P., 1996. Gradient-enhanced damage for quasi-brittle materials. International Journal for Numerical Methods in Engineering 39, 3391–3403.
Pereira, E.M.B.R., Freitas, J.A.T., 2000. Numerical implementation of a hybrid-mixed finite element model for reissner-mindlin plates. Computers & Structures 74, 323–334.
Pijaudier-Cabot, G., Bažant, Z.P., 1987. Nonlocal damage theory. ASCE Journal of Engineering Mechanics 113, 1512–1533.
Silva, C., Castro, L., 2005. Hybrid-mixed stress model for the nonlinear analysis of concrete structures. Computers & Structures 83, 2381–2394.
Silva, C., Castro, L., 2007. Hybrid-displacement (trefftz) formulation for softening materials. Computers & Structures 85, 1331–1342.
Silva, C.M., Castro, L.M.S.S., 2004. Hybrid-mixed stress formulations with continuum damage models. In: Proceedings of the XXV Iberian Latin-American Congress on Computational Methods in Engineering, CILAMCE XXV, Recife (Brazil).
Silva, C.M., Castro, L.M.S.S., 2006. Hybrid-mixed stress formulation using continuum damage models. Communications in Numerical Methods in Engineering 22, 605–617.
Timoshenko, S.P., Goodier, J.N., 1970. Theory of Elasticity, third ed. McGraw-Hill.
Wang, Z., 2000. Elastoplastic structural analysis with hybrid stress elements. PhD thesis, Instituto Superior Técnico, Universidade Técnica de Lisboa, Lisboa.